

## DOWNFLOWS IN SUNSPOT UMBRAL DOTS

A. ORTIZ<sup>1</sup>, L.R. BELLOT RUBIO<sup>2</sup>, AND L. ROUPPE VAN DER VOORT<sup>1</sup>

<sup>1</sup> Institute of Theoretical Astrophysics, University of Oslo, P.O. Box 1029 Blindern, N-0315 Oslo, Norway; ada@astro.uio.no, and

<sup>2</sup> Instituto de Astrofísica de Andalucía (CSIC), Apdo. 3004, 18080 Granada, Spain

Received 2010 February 13; accepted 2010 March 9; published 2010 April 1

### ABSTRACT

We study the velocity field of umbral dots (UDs) at a resolution of  $0''.14$ . Our analysis is based on full Stokes measurements of a pore taken with the Crisp Imaging Spectro-Polarimeter at the Swedish 1 m Solar Telescope. We determine the flow velocity at different heights in the photosphere from a bisector analysis of the Fe I 630 nm lines. In addition, we use the observed Stokes  $Q$ ,  $U$ , and  $V$  profiles to characterize the magnetic properties of these structures. We find that most UD are associated with strong upflows in deep photospheric layers. Some of them also show concentrated patches of downflows at their edges, with sizes of about  $0''.25$ , velocities of up to  $1000 \text{ m s}^{-1}$ , and enhanced net circular polarization signals. The downflows evolve rapidly and have lifetimes of only a few minutes. These results appear to validate numerical models of magnetoconvection in the presence of strong magnetic fields.

*Subject headings:* sunspots — Sun: surface magnetism

### 1. INTRODUCTION

At high angular resolution, sunspot umbrae exhibit small bright features embedded in a darker, smoothly varying background. These features are called umbral dots (UDs) and occur in essentially all sunspots but also in pores (for a review, see Sobotka 1997). Frequently a distinction is made between central and peripheral UD based on their location within the umbra (e.g. Grossmann-Doerth 1986; Riethmüller et al. 2008; Sobotka & Jurčák 2009). Central UD do not show measurable vertical flows and have similar magnetic field inclinations as the surrounding umbra. In contrast, upflows and more horizontal magnetic fields are detected in peripheral UD.

The importance of UD lies in the fact that they may be the signature of convection in sunspots. We know that convective motions must exist because radiation alone cannot explain the brightness of the umbra (Deinzer 1965). The question is whether these motions are field free or magnetized. Recent simulations of magnetoconvection in a strong background field (Schüssler & Vögler 2006) suggest that the convective energy transport inside the umbra is achieved in the form of narrow plumes of rising hot plasma and strongly reduced magnetic fields. The plumes are associated with bright structures that share many similarities with real UD, including their sizes (about 300 km) and lifetimes (30 minutes). The simulated UD tend to be elliptical in shape, and many have a central dark lane.

According to Schüssler & Vögler (2006), the pile-up of material at the top of the plumes increases the gas density and moves the  $\tau = 1$  level toward higher layers, where the temperature is lower. This produces the dark lanes of the simulated UD. The upflows attain maximum velocities of  $3\text{--}4 \text{ km s}^{-1}$  just below the solar surface. Near  $\tau = 1$  they turn horizontal and move in the direction of the dark lane, until the gas returns to deeper layers along narrow channels. The downflows occur mainly at the endpoints of the dark lanes, but also in the immediate surroundings of the UD. They usually appear as tiny patches of concentrated flows with velocities of up to  $1200 \text{ m s}^{-1}$  at  $z = 0 \text{ km}$ . The velocities at  $\tau = 1$  are smaller because the large opacity of the gas hides the layers where the flows are stronger (Bharti et al. 2010).

The simulations of Schüssler & Vögler (2006) suggest that

UD are a natural consequence of convection in a strong magnetic field, which seems to favor the monolithic sunspot model over the cluster model. However, the basic physical process at work in the simulations, namely overturning convection, has not yet been confirmed observationally. Upflows are known to exist in UD; what is missing is a clear, unambiguous detection of return downflows.

The velocity field of UD has been studied by a number of authors. Most of them report negligible velocities in central UD (e.g., Schmidt & Balthasar 1994; Rimmele 2008; Riethmüller et al. 2008; Sobotka & Jurčák 2009) and upflows ranging from  $100 \text{ m s}^{-1}$  to  $1000 \text{ m s}^{-1}$  in peripheral UD (e.g., Socas-Navarro et al. 2004; Rimmele 2004; Riethmüller et al. 2008; Sobotka & Jurčák 2009). Bharti et al. (2007a) claim to have measured upflows of  $400 \text{ m s}^{-1}$  and downflows of  $300 \text{ m s}^{-1}$  in UD, using the Universal Birrefringent Filter at the Dunn Solar Telescope. This is a remarkable result which might have been compromised by the fact that no adaptive optics, phase diversity, or any postprocessing technique such as speckle reconstruction were available at the time of the observations. In any case, the downflows described by Bharti et al. (2007a) seem to be different from those reported by Schüssler & Vögler (2006) in that they extend over much larger areas. The same happens to the downflow patches detected by Bharti et al. (2009) using *Hinode* observations. Interestingly, the spectropolarimetric measurements of Riethmüller et al. (2008) and Sobotka & Jurčák (2009), also from *Hinode*, do not show downward motions despite their better angular resolution ( $0''.3$  versus  $0''.6$ ).

To detect the downflows predicted by the simulations, one would like to have extremely high spatial resolution—higher than typically achieved by current instruments—and line spectra to probe the velocity field at different heights in the atmosphere. Until now it has been difficult to fulfill the two requirements simultaneously. Here, we present the first spectropolarimetric observations of UD approaching a resolution of  $0''.1$ . This unique data set, acquired at the Swedish 1 m Solar Telescope (SST), allows us to investigate the flow field and magnetic properties of UD with unprecedented detail. The measurements show localized patches of downflows at the edges of UD, providing firm evidence for magnetocon-

vection in sunspot umbrae.

The paper is organized as follows. The observations and the data reduction are described in Section 2. Section 3 deals with the morphology, flow field, temporal evolution, and magnetic properties of UDs as derived from the observed Stokes spectra. Finally, in Section 4 we discuss our results and compare them with previous works.

## 2. OBSERVATIONS AND DATA PROCESSING

The observations were obtained with the CRISP Imaging Spectro-Polarimeter (CRISP) at the SST (Scharmer et al. 2003a) on La Palma (Spain). CRISP is based on a dual Fabry Pérot interferometer (FPI) system similar to that described by Scharmer (2006). The instrument has been designed to allow diffraction-limited observations in the visible.

CRISP is equipped with three high-speed Sarnoff CCD cameras operating at 35 frames per second. Two of them are positioned behind the FPI, and the third is located before the FPI but after the CRISP pre-filter. This camera is used as an anchor channel for image processing and is referred to as the wide-band channel. All the cameras take exposures of 17 ms and are synchronized by means of an optical chopper. The image scale is  $0.''071 \text{ pixel}^{-1}$ , and the field of view (FOV) is  $\sim 71'' \times 71''$ . The CRISP transmission profile has an FWHM of 6.4 pm at 630 nm.

The polarization modulation is performed by two nematic liquid crystal (LC) variable retarders cycling through four different states. The time needed to change between LC states is smaller than the CCD read-out time (10 ms) by use of the transient nematic effect. A polarizing beam-splitter in front of the narrow-band cameras divides the light into two orthogonally polarized beams, which results in a significant reduction of seeing-induced cross talk (Lites 1987).

The data analyzed here were recorded on 2008 June 12 and correspond to a pore located at S09 E30 ( $\theta = 31^\circ$ ,  $\mu = 0.85$ ). This pore is the naked umbra of a decaying sunspot (AR 10998) that showed a rudimentary penumbra in previous days. CRISP was used to measure the four Stokes profiles of the Fe I 630.15 and 630.25 nm lines, each sampled at 15 wavelength positions in steps of 4.8 pm, from  $-33.6$  to  $+33.6$  pm. In addition, a continuum wavelength point was observed. CRISP is capable of very fast wavelength tuning ( $\lesssim 50$  ms) within the same spectral region. We recorded 7 exposures per LC state, resulting in 28 exposures per wavelength position. The total time for a complete wavelength scan of the two lines was 26 s.

We followed the pore for 23 minutes during which the atmospheric conditions were variable, with moments of excellent seeing. To improve the spatial resolution, we used the adaptive optics system of the SST (Scharmer et al. 2003b) and the Multi-Object Multi-Frame Blind Deconvolution image restoration technique (MOMFBD; van Noort et al. 2005). All frames in a complete wavelength scan, amounting to 868 images per camera, or 2604 images in total (apart from occasionally dropped frames due to system hick-ups), were included in a MOMFBD restoration. The images were divided into overlapping  $64 \times 64$  pixel subfields ( $4.''5 \times 4.''5$ ) and all images from each subfield were processed as a single MOMFBD set. We refer the reader to van Noort & Rouppe van der Voort (2008) for more details on the MOMFBD processing strategies on similar multi-wavelength polarimetric scans.

The restored images were demodulated (pixel by pixel) and corrected for telescope polarization using the telescope model developed by Selbing (2005). Details on the CRISP polarimetric calibration and the telescope model can be found in

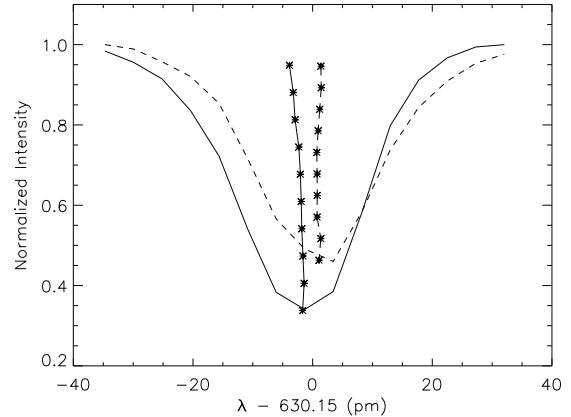


FIG. 1.— Fe I 630.15 nm intensity profiles and line bisectors of UDs showing upflows (solid) and downflows (dotted). The corresponding spatial points are marked with crosses in Figure 2. The profiles have been normalized to their local continua. The bisectors are indicated by asterisks and span the range of intensity levels from 0% to 90%. The 80% bisectors give a velocity of  $-1600 \text{ m s}^{-1}$  for the upflow and  $+810 \text{ m s}^{-1}$  for the downflow.

van Noort & Rouppe van der Voort (2008). After demodulation, the two sets of orthogonal Stokes images recorded by the narrow-band cameras were merged. Precise alignment between these images is ensured by the pinhole calibration performed as part of the MOMFBD processing. The final Stokes profiles were corrected for residual  $I$  to  $Q$ ,  $U$ , and  $V$  crosstalk by forcing the polarization to be zero in the continuum. Another correction was applied to remove the intensity gradient introduced by the CRISP pre filter (FWHM 0.44 nm).

The noise level in Stokes  $Q$ ,  $U$ , and  $V$  amounts to  $2.3 \times 10^{-3}$ ,  $1.6 \times 10^{-3}$ , and  $1.7 \times 10^{-3}$  of the continuum intensity, respectively. This is roughly a factor of 2 higher than the noise level of Scharmer et al. (2008), who used 4 times more exposures. We confirmed that the spatial resolution achieved in our Stokes maps is close to the diffraction limit of the SST by analyzing intensity cuts of the smallest features in the images. We conclude that the spatial resolution is basically limited by the pixel size,  $0.''071$ , which slightly undersamples the theoretical diffraction limit of the telescope ( $\lambda/D = 0.''13$  at 630 nm).

### 2.1. Line parameters

In this work, we use line bisectors to obtain the velocity field of UDs. The bisector is the locus connecting the mid-points of horizontal segments between the two wings of the intensity profile (see Figure 1 for an example). We determined the bisector positions at different intensity levels, from 0% (line core) to 80% (line wing near the continuum), with the help of the `bisec_abs_lin.pro` routine included in the Kiepenheuer-Institut für Sonnenphysik IDL library. The line core position was computed by means of a parabolic fit around the intensity minimum. The calculations were performed only for Fe I 630.15 nm, since the red wing of Fe I 630.25 nm is blended with a telluric  $\text{O}_2$  line. The bisector positions were converted into Doppler velocities assuming that the pore is at rest. More specifically, we averaged the bisectors between the 40% and 70% intensity levels within the pore and took this as the zero point of the velocity scale. The rms fluctuation of the velocity in the pore is  $320 \text{ m s}^{-1}$ , as computed from the 80% bisector. This is larger than the values reported by Franz & Schlichenmaier (2009), which we attribute to the higher spatial resolution of our observations and the fact

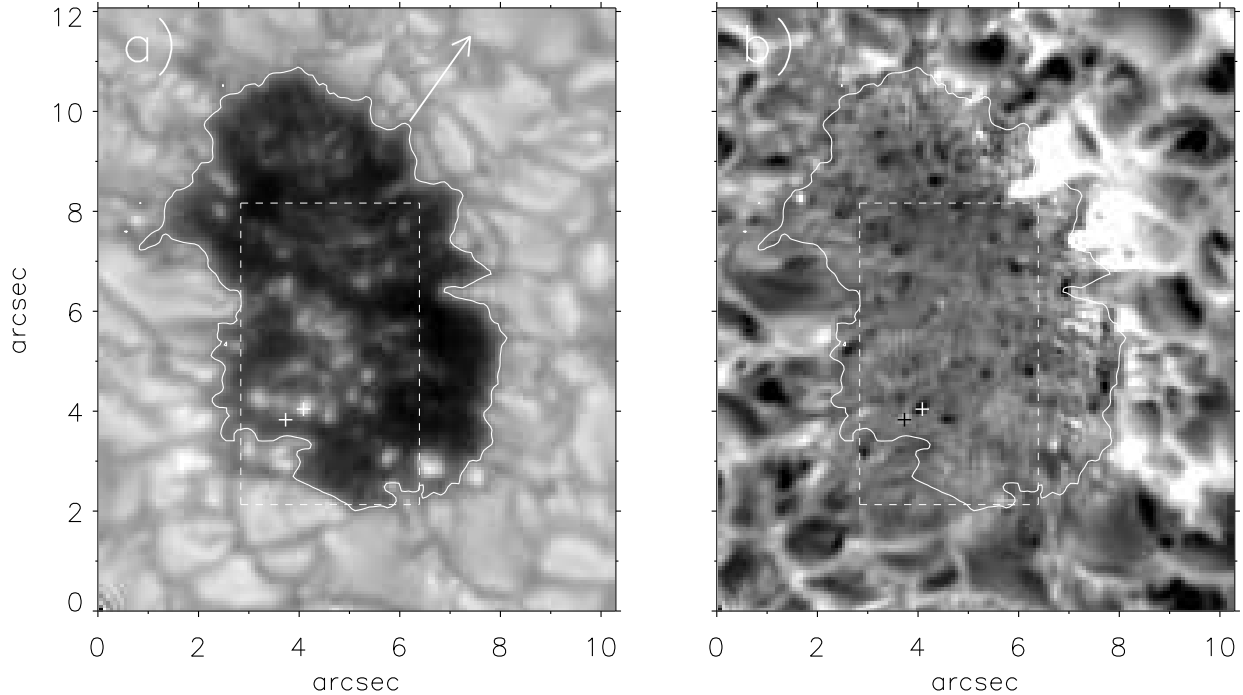


FIG. 2.— AR 10998 as observed by CRISP on 2008 June 12 at 10:33 UT. (a) Continuum intensity image from the narrow band channel of CRISP. The contours outline the edge of the pore and the arrow marks the direction to disk center. The rectangle encloses the region studied in Figure 3. Note the complex network of magnetoconvective structures inside the pore. There are UDs with and without dark lanes. (b) LOS velocity map computed from the bisector position at the 80% intensity level. The gray scale ranges from  $-1.5 \text{ km s}^{-1}$  (black) to  $1.5 \text{ km s}^{-1}$  (white). Negative velocities indicate blueshifts.

that we see clear flow structures embedded in the dark umbral background. The systematic error of such a velocity calibration is not larger than about  $150 \text{ m s}^{-1}$  (Rezaei et al. 2006).

The availability of spectrally resolved line profiles makes it possible to probe the velocity field at different heights in the photosphere. Roughly speaking, higher intensity levels correspond to deeper layers. The continuum is formed at around  $\log \tau = 0$ , whereas the Fe I 630.15 nm line core is formed at  $\log \tau = -2.9$  in the quiet Sun, according to Balthasar (1985). These values are consistent with the difference of approximately 270 km reported by Grec et al. (2010) between the formation heights of the continuum and the line core of Fe I 630.15 nm. It is important to realize, however, that the intensity observed at a given wavelength is affected by the conditions of a large fraction of the atmosphere (e.g., Cabrera Solana et al. 2005, and references therein). Thus, any formation height actually represents a broad range of optical depths.

To investigate the magnetic properties of UDs we use simple line parameters derived from the observed Stokes  $Q$ ,  $U$ , and  $V$  profiles. These are the mean linear polarization (LP) degree,

$$\text{LP} = \frac{\int_{\lambda_b}^{\lambda_r} [Q^2(\lambda) + U^2(\lambda)]^{1/2} / I(\lambda) d\lambda}{\int_{\lambda_b}^{\lambda_r} d\lambda}, \quad (1)$$

the mean circular polarization (CP) degree,

$$\text{CP} = \frac{\int_{\lambda_b}^{\lambda_r} [V(\lambda)] / I(\lambda) d\lambda}{\int_{\lambda_b}^{\lambda_r} d\lambda}, \quad (2)$$

and the net circular polarization (NCP),

$$\text{NCP} = \int_{\lambda_b}^{\lambda_r} V(\lambda) d\lambda / I_c. \quad (3)$$

Here,  $\lambda_r$  and  $\lambda_b$  represent the limits of integration over the line, and  $I_c$  is the continuum intensity. The NCP accounts for the asymmetries in the Stokes  $V$  profile, which are due to gradients in the magnetic field and the line-of-sight (LOS) velocity (Illing et al. 1975; Auer & Heasley 1978).

In addition, we have determined the longitudinal component of the magnetic field using the center-of-gravity (COG) method (Rees & Semel 1979; Landi degl'Innocenti & Landolfi 2004). The LOS component of the field is obtained through the relation

$$B_{\text{LOS}} = \frac{(\lambda_+ - \lambda_-) / 2.0}{4.67 \times 10^{-13} g_L \lambda_0^2}, \quad (4)$$

where  $g_L$  is the Landé factor,  $\lambda_0$  is the central wavelength of the line in  $\text{\AA}$ , and  $\lambda_{\pm}$  are the centroids of the right and left circularly polarized line components ( $I \pm V$ ), calculated as

$$\lambda_{\pm} = \frac{\int \lambda [I_c - (I \pm V)] d\lambda}{\int [I_c - (I \pm V)] d\lambda} \quad (5)$$

(Uitenbroek 2003). The COG method is not affected by saturation effects in the strong field regime.

The inclination  $\gamma$  of the magnetic field vector with respect to the LOS is determined as

$$\gamma = \arccos \frac{\sqrt{1+x^2}-1}{x}, \quad (6)$$

where

$$x = \frac{V}{\sqrt{Q^2 + U^2}}. \quad (7)$$

This expression is valid for fully split lines (Landi degl'Innocenti & Landolfi 2004). We apply Equation (6) to six wavelength samples around the peaks of the Stokes  $V$  profile (three in the red lobe and another three in the

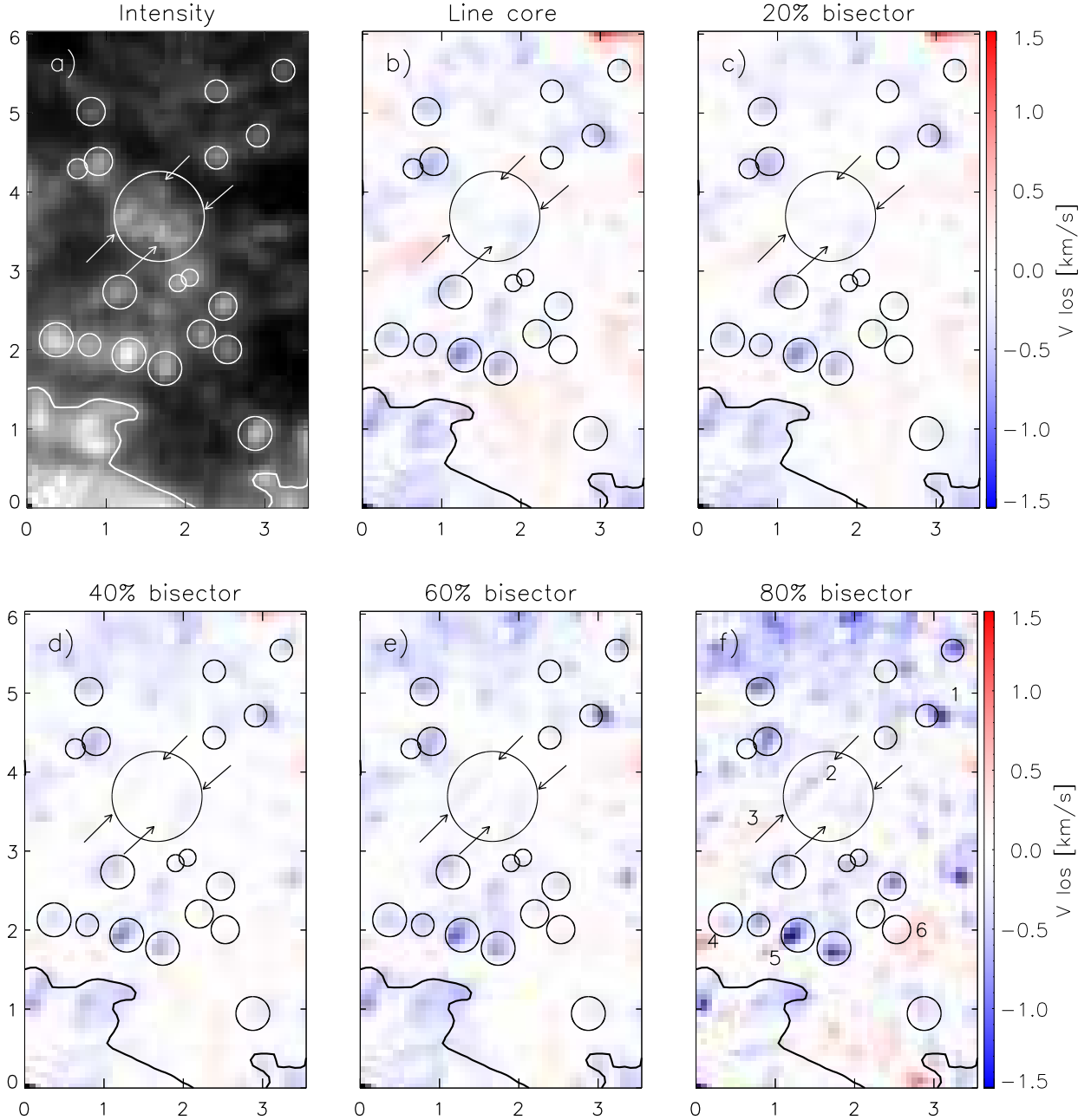


FIG. 3.— LOS velocities in an area of the pore with high density of UDs (see the rectangle in Figure 2). Distances are measured in arcsec. The contour lines indicate the edge of the pore. (a) Continuum intensity image. (b)-(f) Velocity maps at intensity levels from 0% to 80%. The circles enclose selected UDs and the numbers refer to the downflow patches considered in Table 1.

blue lobe) and take the mean. Once  $B_{\text{LOS}}$  and  $\gamma$  are known, the magnetic field strength  $B$  is obtained as

$$B = B_{\text{LOS}} / |\cos \gamma|. \quad (8)$$

To reduce the noise, the line parameters LP, CP, and NCP, as well as the magnetic field parameters  $B_{\text{LOS}}$ ,  $\gamma$ , and  $B$ , have been computed separately for the two lines and then averaged.

### 3. RESULTS

#### 3.1. Morphological properties

Figure 2(a) displays a continuum image of the pore as observed on 2008 June 12 at 10:33 UT. The direction to disk

center is indicated by the arrow. The pore covers an area of around  $6'' \times 9''$  and shows a complex network of magnetoconvective structures (UDs) of different sizes, shapes, and brightnesses. In general bigger structures are found in the lower half of the pore. Some of the observed UDs present a dark lane along their axis. Two of them even resemble *coffee beans* because of their conspicuous dark lanes; one is located at  $(x, y) = (4'', 6'')$  and the other at  $(x, y) = (5'', 5''.5)$ . These two specific UDs have a size of  $0''.7$  and the smallest dark lane is  $0''.14$  in width (probably unresolved), in agreement with Rimmele (2008) and Sobotka & Puschmann (2009). Smaller UDs without a dark lane have a typical diameter of  $0''.3$  and minimum sizes of less than  $0''.2$ .

TABLE 1  
Downflows Observed in Selected UDs

Patch	Size	Distance	$v_{\text{LOS}}$ ( $\text{m s}^{-1}$ )	Distance	$v_{\text{LOS}}$ ( $\text{m s}^{-1}$ )	UD size	$I_{\text{max}}/I_{\text{QS}}$
1	$0''.21 \times 0''.21$	$0''.21$	580	$0''.14$	-1150	$0''.21 \times 0''.14$	0.71
2	$0''.21 \times 0''.21$	$0''.28$	680	$0''$	-620	$0''.70 \times 0''.35$	0.94
3	$0''.70 \times 0''.21$	$0''.14$	440	$0''$	-620	$0''.70 \times 0''.35$	0.94
4	$0''.28 \times 0''.28$	$0''.21$	990	$0''$	-380	$0''.28 \times 0''.35$	1.07
5	$0''.28 \times 0''.14$	$0''.28$	650	$0''.07$	-1420	$0''.28 \times 0''.28$	1.19
6		$0''$	520			$0''.21 \times 0''.21$	0.78

NOTE. — Column 1: number of downflow patch in Figure 3(f). Column 2: size of downflow patch. Column 3: distance of downflow patch to UD intensity maximum. Column 4: downflow velocity at the 80% intensity level. Column 5: distance of upflow patch to UD intensity maximum. Column 6: upflow velocity at the 80% intensity level. Column 7: size of UD. Column 8: UD intensity maximum, normalized to the average quiet Sun continuum intensity.

### 3.2. Velocity field

The main goal of this work is to obtain the velocity field of the UDs present in the pore. Figure 2(b) shows the LOS velocities derived from the bisector at the 80% intensity level. The gray scale is clipped at  $\pm 1.5 \text{ km s}^{-1}$  to emphasize the weaker flows. Negative velocities indicate blueshifts. Given the heliocentric angle of the observations and the fact that the magnetic field is nearly vertical, blueshifts most probably represent upflows and redshifts downflows.

The granulation pattern is clearly visible, while the pore shows a complex network of small-scale flow elements. One of the striking features of this map is the strong downflows seen at the very edge of the pore, near  $(x, y) = (7'', 9'')$ . They will be explored in a forthcoming publication. Most of the umbra has small velocities close to zero, but one can detect the presence of many upflows and some downflow patches inside the pore. These structures are located at the position of the UDs observed in Figure 2(a), with small deviations that we will discuss later. The upflows reach up to  $-1400 \text{ m s}^{-1}$ , while the downflows show a more modest value of around  $400\text{--}1000 \text{ m s}^{-1}$  at the 80% intensity level.

Figure 3 displays the velocity field within the boxed area of Figure 2. For convenience, panel (a) shows the corresponding continuum image. The circles mark selected UDs, and are centered at the position of maximum brightness. The arrows indicate the two UDs with dark lanes. Panels (b)–(f) show the bisector velocities at five intensity levels, from 0% to 80%. In this way, we probe different layers of the photosphere.

The bisectors close to the line core reveal small Doppler shifts. The upflows and downflows associated with the UDs become gradually stronger toward the continuum, such that the larger velocities are seen at the 80% intensity level [Figure 3(f)]. Thus, the flows occur preferentially in deep photospheric layers, and a gradient of velocity with height appears to exist. Such a gradient may partly explain the difficulty of detecting flows in UDs; it is common to use the line core for velocity determinations, but these measurements probe too high layers already devoid of flows.

The majority of UDs show upflows, with maximum velocities of around  $1400 \text{ m s}^{-1}$  at the 80% intensity level. The average size of the upflow patches is around  $0''.25$ , slightly smaller than the UDs themselves. It is interesting to note that the location of the upflow do not always exactly overlap with the position of maximum brightness of the corresponding UD. Displacements of  $0''.07\text{--}0''.14$  (1–2 pixels) are common at all intensity levels. This is best seen in Figure 3(f),

where the photometric centers of the UDs and the associated blue patches tend to be shifted, although the flows always remain inside the circles representing the UDs.

Downflows are observed in some UDs, but almost exclusively at the 80% intensity level<sup>1</sup>. In those deep layers, they tend to appear at the edges of UDs exhibiting upflows. However, we note that not all UDs with upflows have an associated downflow. Part of this may be due to their transient nature (Section 3.3). In the case of the UDs showing a dark lane, the upflows are cospatial with the dark lane and the downflows occur at the endpoints.

The properties of some selected downflows are presented in Table 1. The numbers in the first column identify the corresponding patches in Figure 3(f). All of them are related to an adjacent upflow, except for patch 6 which does not seem to be associated with any measurable upflow (this patch is embedded in a large area of redshifts, so it may not be typical). The properties of the upflows are given in Table 1 along with those of the parent UDs. The average size of the downflow patches is about  $0''.25$ , but elongated areas of up to  $0''.7$  also exist. Since the downflows occur at the periphery of UDs, they can be shifted by as much as  $0''.28$  (4 pixels) from the position of maximum brightness. There seems to be a preferred direction of displacement which coincides with the line of symmetry (i.e., the direction to disk center), even though not in all cases, since patch 6 does not follow that direction. The displacements might simply reflect an enhanced visibility of the downflows near the line of symmetry due to projection effects. The LOS velocities range from  $400 \text{ m s}^{-1}$  to almost  $1000 \text{ m s}^{-1}$  at the 80% intensity level. We do not find any relationship between the area of the downflow patch and its velocity (patch 4, with the highest measured velocity, is not particularly big or small), or between the area and the distance to the UD in continuum intensity.

### 3.3. Temporal evolution

We have also studied the temporal evolution of the UDs inside the pore. Their morphological properties change rapidly with time. This is demonstrated in Figure 4, where six snapshots covering the period from 10:28 UT to 10:49 UT are presented. The upper, middle, and lower panels show continuum images, velocity maps derived from the 80% bisector,

<sup>1</sup> The extended areas of weak redshifts seen in the line core map coincide with the darkest parts of the umbra, so they are not related to UDs. The redshifts could be produced either by oscillations or by downward motions of the pore as a whole.

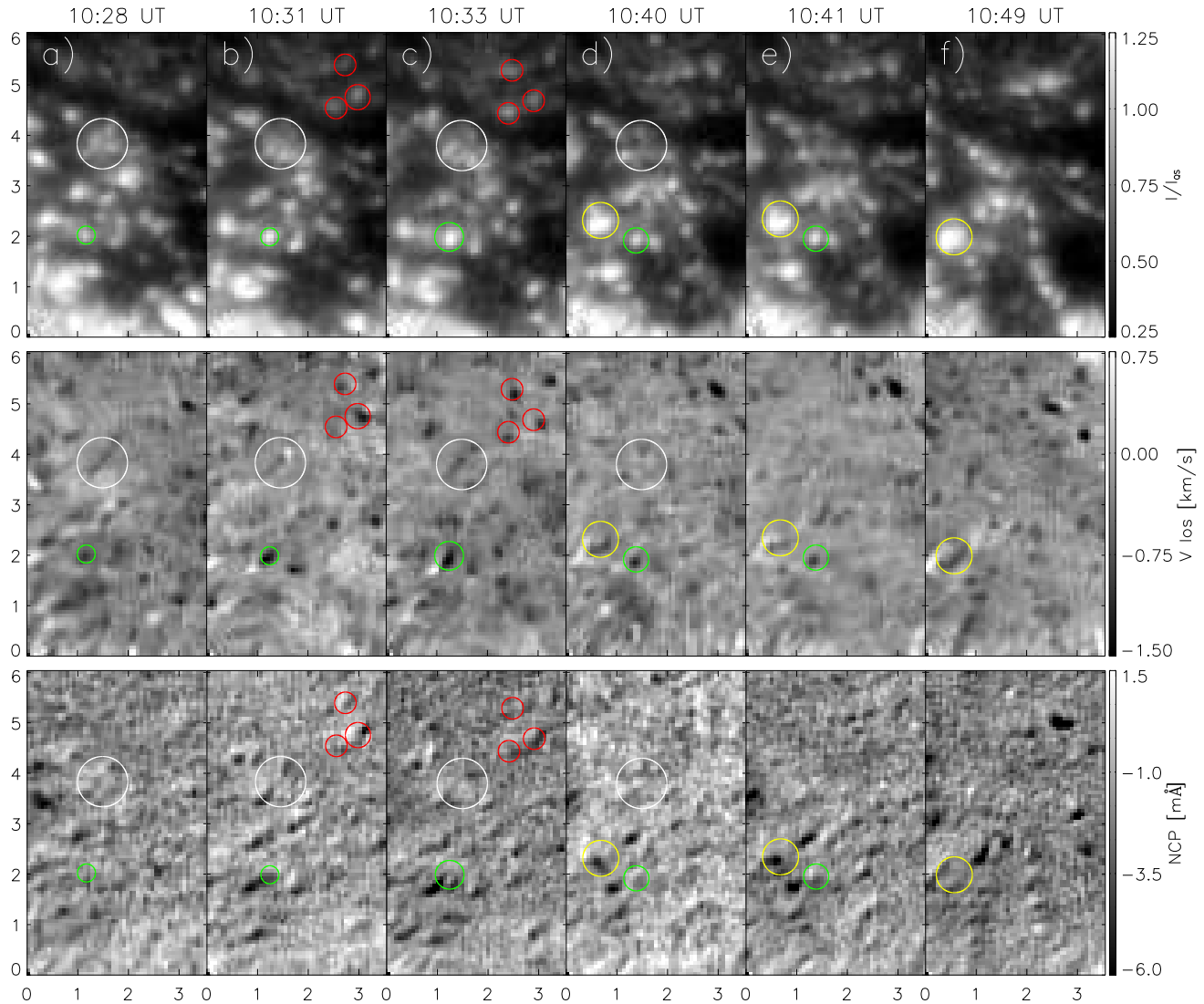


FIG. 4.— Temporal evolution of UDs in AR 10998. Panels (a)-f) show six snapshots taken between 10:28 and 10:49 UT on 2008 June 12. Marks have been made every arcsecond. The upper panels show continuum images zooming in the same area as Figure 3. The middle and lower panels display velocity maps derived from the 80% bisector and NCP maps. The evolution of the UDs indicated by the circles is discussed in the text.

and NCP maps, respectively. The circles mark prototypical UDs whose evolution we have followed in more detail.

The green circles trace the evolution of a small UD in the lower half of the pore. The apparent size of this UD changes from a diameter of  $0''.3$  at 10:28 UT to  $0''.5$  at 10:33 UT, as seen in continuum intensity. Not only does the diameter vary, but also the velocity. This particular UD is interesting because it harbors both strong upflows and downflows during part of its existence. It starts showing an upflow of  $-950 \text{ m s}^{-1}$ , but no downflow. At 10:31 UT the upflows have increased to  $-1530 \text{ m s}^{-1}$ , and a downflow patch of around  $700 \text{ m s}^{-1}$  has appeared next to the upflow patch. At 10:33 UT the upflows are the same while the downflows have increased to  $820 \text{ m s}^{-1}$ . At 10:40 and 10:41 UT, the motions seem to slow down, reaching velocities of  $-950 \text{ m s}^{-1}$  and  $180 \text{ m s}^{-1}$ , respectively. The sizes of the upflow and downflow patches do not change much in this particular example.

At 10:49 UT, a fast downflow of  $950 \text{ m s}^{-1}$  becomes very prominent in the lower left part of the image (yellow circles).

This patch had existed at least during three snapshots, but it is in the last one when it shows the highest velocities. The downflows have the shape of a collar surrounding a large UD with upflows of  $-780 \text{ m s}^{-1}$ .

The red circles pinpoint a group of three UDs in the upper part of the FOV. They are well visible at 10:31 and 10:33 UT but have already disappeared at 10:40 UT. At 10:31 UT, the rightmost UD shows an upflow of  $-1280 \text{ m s}^{-1}$  and an adjacent downflow of  $470 \text{ m s}^{-1}$ . The other two UDs harbor upflows of  $-950 \text{ m s}^{-1}$  on average. At 10:33 UT, the downflow patch has vanished and the upflows have decreased to  $-1150 \text{ m s}^{-1}$ .

Finally, the white circles highlight one of the UDs that contain a dark lane. The dark lane appears in intensity at 10:31 UT and disappears at 10:40 UT as the whole structure becomes blurry. In the velocity maps, we can observe narrow, elongated upflows that coincide with the position of the dark lane. Their velocities are  $-670 \text{ m s}^{-1}$  at 10:28 UT,  $-730 \text{ m s}^{-1}$  at 10:31 UT, and  $-860 \text{ m s}^{-1}$  at 10:33 UT. At 10:31 UT, down-

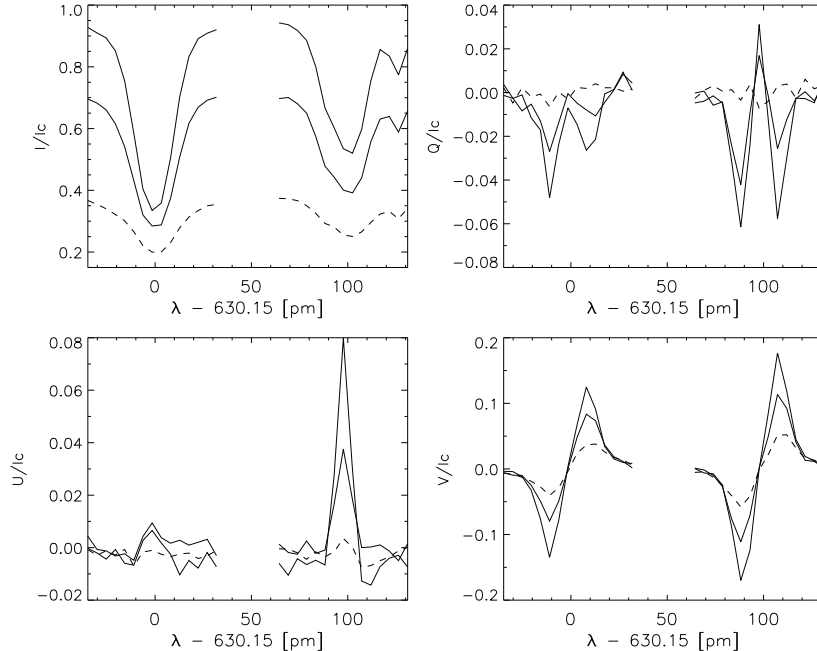


FIG. 5.— Stokes  $I$ ,  $Q$ ,  $U$ , and  $V$  profiles emerging from a UD (solid line), its dark lane (thick solid line), and the adjacent umbra (dashed line). The profiles are normalized to the quiet Sun continuum intensity.

flow patches of  $560 \text{ m s}^{-1}$  appear at the two endpoints of the dark lane. One of the patches is as small as  $0''.14$  in diameter. Their velocities quickly decrease with time; 2 minutes later, at 10:33 UT, the downflows are no longer visible.

All of these cases corroborate: (1) the ephemeral life of the UDs themselves (around 10 minutes), (2) the ephemeral life of their substructures (the dark lanes are well defined for only around 4 minutes), and (3) the quick change in their velocities, with upflow/downflow motions lasting only for a few minutes. In fact, Sobotka & Puschmann (2009) report that the substructures observed within UDs (i.e., the dark lanes) vary with a typical time scale of about 3 minutes. According to Sobotka & Puschmann (2009), dark lanes disappear and reappear during the evolution of central UDs. Our time sequence is relatively short, and we have been unable to observe the reappearance of any dark lane.

#### 3.4. Polarization signals and magnetic properties

In Figure 5, we present the four Stokes profiles of an UD, its dark lane, and the surrounding umbra. The selected UD is the one enclosed by the white circle in Figure 4. With a continuum approaching that of the quiet Sun, this UD is brighter than the adjacent umbra by a factor of about 2.6. Sobotka et al. (1993) deduced that the brightness of UDs is at most 3 times that of the background umbra. Our observations appear to confirm this result, derived from a careful analysis of high-resolution photometric measurements. A factor of 2.6 is also in agreement with the average continuum ratio of 2.58 obtained from magnetoconvection simulations at 630 nm (Bharti et al. 2010). The dark lane, in turn, is observed to be about 25% darker than the brightest part of the UD.

The UD and the dark lane show significantly larger Stokes  $V$  signals than the umbral background. Socas-Navarro et al. (2004) pointed out that this does not imply stronger magnetic fields, but is just a consequence of a steeper source function gradient in hot structures. The UD and the dark lane also show enhanced Stokes  $Q$  and  $U$  signals, suggesting more inclined

fields. Overall, the spectra displayed in Figure 5 are very similar to those presented by Socas-Navarro et al. (2004), except that these authors did not resolve the contribution of the dark lane.

Figure 6 shows maps of circular and linear polarization signals, NCPs, field strengths, and field inclinations in the pore. The circles indicate selected UDs, and the dark lanes are named DL1 and DL2.

In linear polarization, the UDs stand out clearly above the umbral background. The umbra has weak signals due to its nearly vertical fields and the small heliocentric angle of the observations. UDs 5 and 7 get the higher LP values among the selected UDs. Interestingly, the dark lanes DL1 and DL2 exhibit smaller degrees of linear polarization than their corresponding UDs. In circular polarization, the UDs are also the most prominent features, despite the fact that the umbral background is now very intense. The dark lanes again show smaller signals than their UDs.

It is remarkable that many UDs have strong negative NCPs. The temporal evolution of those signals is displayed in the lower panels of Figure 4. The NCP patches are shifted with respect to the photometric center of the UDs, and tend to coincide with downflow areas (e.g., UD4 and UD5) or with the border of an upflow patch (e.g., UD6). The dark lanes exhibit nearly zero NCPs, but the downflows at their endpoints sometimes show large negative values (e.g., DL2). The asymmetries of Stokes  $V$  provide us with valuable information. As discussed by Solanki & Montavon (1993), the sign of the NCP is determined by the following rules:

$$\text{sign}(\text{NCP}) = -\text{sign} \left( V_{\text{blue}} \frac{dv_{\text{LOS}}}{d\tau} \frac{dB}{d\tau} \right), \quad (9)$$

$$\text{sign}(\text{NCP}) = -\text{sign} \left( V_{\text{blue}} \frac{dv_{\text{LOS}}}{d\tau} \frac{d|\cos \gamma|}{d\tau} \right), \quad (10)$$

where  $V_{\text{blue}}$  represents the sign of the blue lobe of Stokes  $V$  (negative in our case),  $B$  is the magnetic field strength (pos-

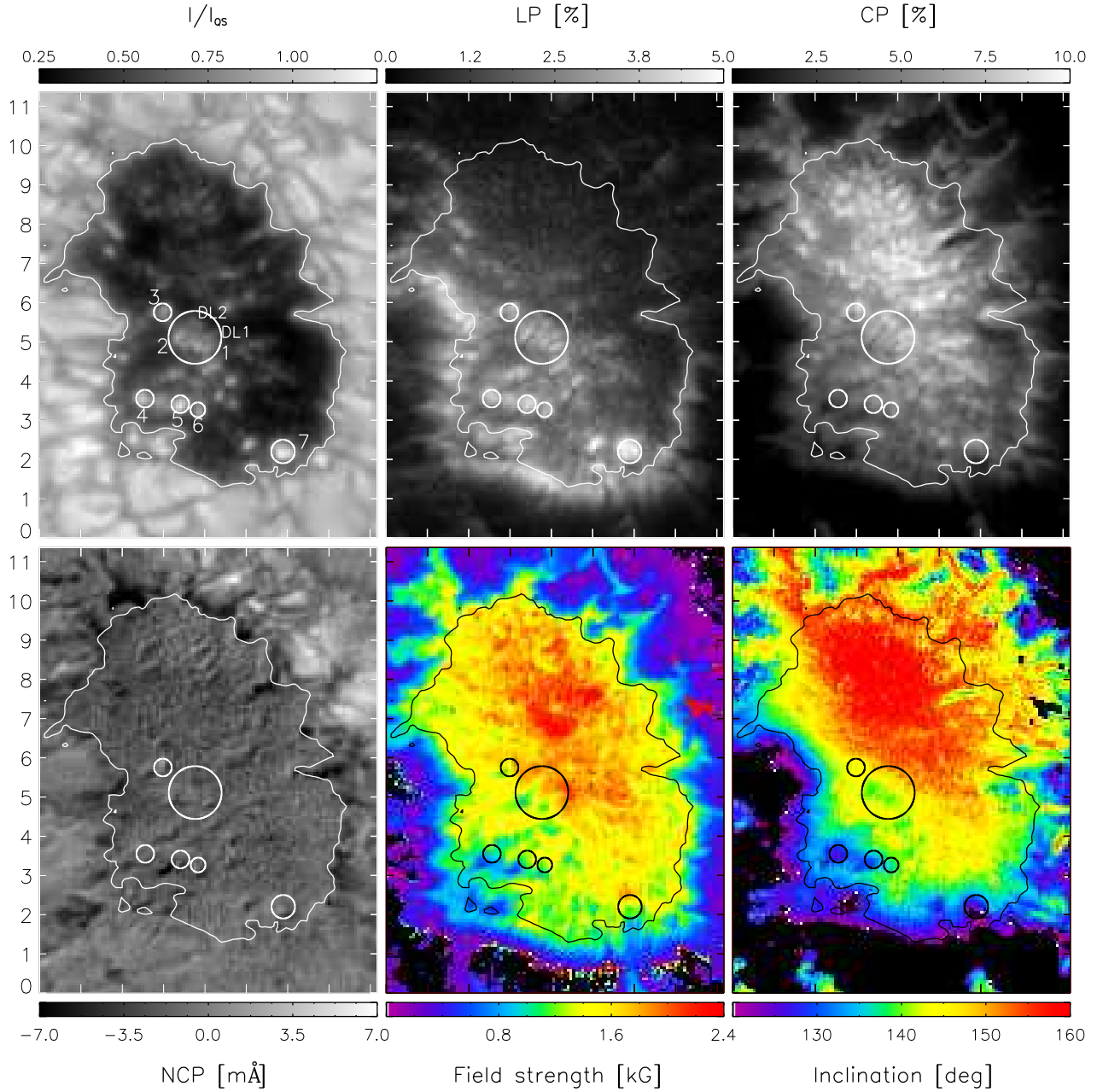


FIG. 6.— Magnetic properties of UDs. In all panels we have marked the edges of the pore with contour lines and a few UDs with circles. Tickmarks are separated by  $1''$ . *Top*: continuum image of the pore and its magnetoconvective structures (left); mean linear polarization degree (middle); mean circular polarization degree (right). *Bottom*: net circular polarization (left); magnetic field strength (middle); magnetic field inclination (right).

itive by definition), and  $v_{\text{LOS}}$  is positive for downflows and negative for upflows. We expect larger changes of  $B$  with height than of  $\gamma$ , hence the first relation above is likely to set the NCP sign. The NCP patches coincide with downflows for the most part. Since the bisector velocities increase toward the continuum,  $dv_{\text{LOS}}/d\tau > 0$  in those areas. Thus, to produce a negative NCP it is necessary that  $dB/d\tau$  be negative, i.e., the magnetic field strength must decrease as the optical depth increases. This result lends support to the idea that UDs are structures with significantly reduced fields near or just below the continuum forming layers.

The interpretation of the observed polarization signals is difficult because of the interplay of the various atmospheric parameters and the existence of thermal effects. The field

strength and inclination maps of Figure 6, however, show that many UDs are associated with weaker and slightly more inclined fields than their surroundings. The dark lanes have even weaker fields. The areas of weaker fields seem to coincide in general with the locations of downflows but not with upflows (the dark lanes are an exception, showing both upflows and weaker fields). In the simulations, the downflows of the largest UDs are sometimes associated with reversed magnetic polarities, but only near  $\tau = 1$  (Bharti et al. 2010). We do not observe opposite-polarity fields in our observations.

Table 2 quantifies the properties of the UDs marked in Figure 6. To allow comparisons, we also give the properties of nearby points in the umbral background (UB). The magnetic field strength of the UDs is considerably weaker than that



TABLE 2  
Magnetic Properties of Selected UDs

Structure	B (G)	$\gamma$ ( $^\circ$ )	LP (%)	CP (%)	NCP (mÅ)
UD1	1610	139	4.0	9.8	-1.5
DL1	1220	141	3.2	8.1	-0.5
UB1	1900	150	2.1	8.2	-0.4
UD2	1500	138	3.8	9.3	-3
DL2	1020	141	2.8	7.4	0.8
UB2	1800	142	2.1	7.0	-0.8
UD4	800	124	4.1	5.0	-4
UB4	1200	134	2.5	5.0	-1.5
UD5	1190	129	4.4	7.4	-9
UB5	1140	140	2.2	5.0	-2
UD6	1280	138	3.7	6.9	-4
UB6	1450	141	2.2	5.8	-2.7
UD7	1070	121	4.9	6.0	-3
UB7	1480	140	2.3	5.6	-1.2

NOTE. — Column 1: number of UD and adjacent UB in Figure 6. Column 2: magnetic field strength. Column 3: inclination of magnetic field vector to the LOS. Column 4: mean linear polarization degree. Column 5: mean circular polarization degree. Column 6: net circular polarization.

of the umbra, which peaks at about 2400 G. Differences are smaller when the comparison is made with the immediate UB. In some cases, like UD4, the magnetic field is as weak as 800 G. The dark lanes are the regions with weaker fields within the UDs: DL1 and DL2 show strengths of 1000–1200 G, while the bright parts of the corresponding UDs have fields of some 1500–1600 G. In the umbra, the field is inclined to the LOS by up to  $160^\circ$ , as expected for vertical fields at an heliocentric angle of  $\sim 30^\circ$ . By contrast, the UDs exhibit inclinations closer to  $90^\circ$  and thus possess more horizontal fields. UDs 4 and 7 in particular have the largest inclinations ( $124^\circ$  and  $121^\circ$ , respectively), perhaps because of their location near the edge of the pore. Compared with the adjacent background, UDs show inclination differences of  $3^\circ$ – $17^\circ$ . The dark lanes have similar inclinations as their UDs, but higher than other unresolved UDs.

In summary, UDs exhibit weaker magnetic fields than the surrounding umbra as well as more inclined field lines. These results confirm previous works (e.g. Socas-Navarro et al. 2004; Riethmüller et al. 2008; Sobotka & Jurčák 2009). The new information here is that of the dark lanes, whose magnetic properties have not been determined earlier. We report that the dark lanes exhibit an even weaker magnetic field than their associated UDs, up to 500 G less, as well as smaller LP, CP, and NCP signals. The field inclination, however, does not differ from that of the UDs. Another new result is the existence of enhanced NCP in the downflow patches observed at the periphery of UDs. The sign of the NCP indicates that the field strength decreases with depth in the photosphere.

#### 4. DISCUSSION AND CONCLUSIONS

We have presented the first spectropolarimetric measurements of UDs at a resolution of  $0''.14$ . Our observations reveal the existence of substructures within UDs in the form of dark lanes. Only Bharti et al. (2007b), Rimmele (2008), and Sobotka & Puschmann (2009) have detected these structures before. Rimmele (2008) estimated their size to be  $0''.12$  in G-band images, right at the diffraction limit of the Dunn Solar Telescope, while Sobotka & Puschmann (2009) reported widths of less than  $0''.14$  from broadband 602 nm filtergrams taken at the SST. Our observations also indicate sizes of  $0''.14$ .

At the resolution of CRISP, however, not all UDs possess a dark lane.

In this paper, we have focused on the velocity field of UDs. One can find in the literature a variety of works describing the morphological properties of UDs, but very few attempts have been made to determine their velocities. However, very few attempts have been made to determine their velocities. A good knowledge of the flow field of UDs is important both to understand the energy transport in strongly magnetized media and to discern between models of sunspot structure.

Measuring UD velocities is a difficult task, as recognized by several authors (e.g., Rimmele 2004; Socas-Navarro et al. 2004; Schüssler & Vögler 2006). Our results, and those from previous works, point to the existence of large LOS velocities and reduced magnetic field strengths, but only in deep layers of the photosphere –near the continuum forming region– definitely deeper than the layers traced by the core of many photospheric lines. For example, Rimmele (2004) finds upflows of more than  $1 \text{ km s}^{-1}$  in the C I 538.0 nm line (whose core forms at approximately 40 km), while he observes velocities of less than  $300 \text{ ms}^{-1}$  in Fe I 557.6 nm (formation height of around 320 km). Schüssler & Vögler (2006) also mention the difficulty of observing flows and reduced field strengths in UDs because the surfaces of equal optical depth are locally elevated. Other factors such as the small sizes and the rapid evolution of these structures complicate the determination of their velocities and magnetic fields.

Observational studies have found upflows of  $100 \text{ ms}^{-1}$  (Socas-Navarro et al. 2004),  $600 \text{ ms}^{-1}$  (Sobotka & Jurčák 2009),  $800 \text{ ms}^{-1}$  (Riethmüller et al. 2008), and even  $1000 \text{ ms}^{-1}$  (Rimmele 2004) in peripheral UDs. Our data confirm the existence of relatively strong upflows of around  $1000 \text{ ms}^{-1}$ , with peaks up to  $1500 \text{ ms}^{-1}$ . The upward velocities observed in MHD simulations do not exceed  $2000 \text{ ms}^{-1}$  at photospheric levels (Bharti et al. 2010).

The most relevant and novel result of this paper is the finding of *downflows* at the edges of some UDs. If the UD has a dark lane, then the downflows are observed at its endpoints. The downflow velocities range from  $400 \text{ ms}^{-1}$  to almost  $1000 \text{ ms}^{-1}$ . The existence of downflows seems to fit the scenario proposed by Schüssler & Vögler (2006), in which UDs are the result of magnetoconvection in regions of reduced field strengths with both upflows and return downflows. We believe this is the first time that the predicted downflows are reliably measured within UDs, mostly as a consequence of the high resolution provided by CRISP and the SST. We have also examined the LOS velocities at different intensity levels. Since the 80% intensity level shows the strongest velocities and motions at other intensity levels are gradually of lesser magnitude, a gradient of velocity with height appears to exist. This suggests that the flows occur preferentially in the deep layers of the photosphere.

A comparison between our Figure 3(f) and Figure 1(b) of Schüssler & Vögler (2006) reveals some similarities, like the fact that the upflows are co-located with the centers of the UDs and their dark lanes. Also in good agreement is the fact that the downflows are observed around the UD structure, but most prominently at the endpoints of the dark lanes. However, our measured velocities appear to be slightly larger than those predicted by the simulations (see, e.g., Figure 16 of Bharti et al. 2010). In the same manner, the temporal evolution shown in our Figure 4 may be compared with Figure 5 of Schüssler & Vögler (2006), where the highly dynamic and transient nature of the UDs can be seen.

We have also determined the magnetic properties of UDs. New in this work is the description of the properties of their substructure, the dark lanes. UDs exhibit weaker magnetic fields and more inclined field lines than the surrounding umbra, confirming previous analyses (e.g. Socas-Navarro et al. 2004; Riethmüller et al. 2008; Sobotka & Jurčák 2009). We report a magnetic field weakening of up to 500 G between UDs and their adjacent umbral background, similar to the values given by Riethmüller et al. (2008). According to our data, the magnetic field in the UDs is more horizontal than in the immediate surroundings by as much as  $\sim 20^\circ$ . Before this work, the magnetic properties of the dark lanes were largely unknown. We report that they exhibit an even weaker field than their associated UDs, up to 500 G less. The dark lanes also show smaller linear and circular polarization signals. Their inclinations, however, do not differ from those of the associated UDs. Another new result is the existence of enhanced NCP in UDs. We observe tiny patches of NCP that tend to coincide with the downflowing areas. In those regions,

the NCP sign indicates a reduction of the field strength towards deeper photospheric layers. This again appears to confirm the results of numerical simulations (Schüssler & Vögler 2006).

We are grateful to Héctor Socas Navarro for valuable discussions. Part of this work was carried out while one of us (A. O.) was a Visiting Scientist at the Instituto de Astrofísica de Andalucía. This research has been supported by the Spanish Ministerio de Ciencia e Innovación through projects ESP2006-13030-C06-02 and AYA2009-14105-C06-06, by Junta de Andalucía through project P07-TEP-2687, and by the Research Council of Norway through grant 177336/V30. The Swedish 1 m Solar Telescope is operated by the Institute for Solar Physics of the Royal Swedish Academy of Sciences in the Spanish Observatorio del Roque de los Muchachos of the Instituto de Astrofísica de Canarias. This research has made use of NASA's Astrophysical Data System.

#### REFERENCES

- Auer, L. H., & Heasley, J. N. 1978, *A&A*, 64, 67  
 Balthasar, H. 1985, *Sol. Phys.*, 99, 31  
 Bharti, L., Beeck, B., & Schüssler, M. 2010, *A&A*, 510, A12  
 Bharti, L., Jain, R., & Jaaffrey, S.N.A. 2007a, *ApJ*, 665, L79  
 Bharti, L., Joshi, C., & Jaaffrey, S. N. A. 2007b, *ApJ*, 669, L57  
 Bharti, L., Joshi, C., Jaaffrey, S. N. A., & Jain, R. 2009, *MNRAS*, 393, 65  
 Cabrera Solana, D., Bellot Rubio, L. R., & del Toro Iniesta, J. C. 2005, *A&A*, 439, 687  
 Deinzer, W. 1965, *ApJ*, 141, 548  
 Franz, M., & Schlichenmaier, R. 2009, *A&A*, 508, 1453  
 Grec, C., Uitenbroek, H., Furobert, M., & Aime, C. 2010, *A&A*, in press  
 Grossmann-Doerth, U. 1986, *A&A*, 156, 347  
 Illing, R. M. E., Landman, D. A., & Mickey, D. L. 1975, *A&A*, 41, 183  
 Landi degl'Innocenti, E. & Landolfi, M. 2004, *Polarization in Spectral Lines*, Astrophysics and Space Library, Dordrecht: Kluwer  
 Lites, B. W. 1987, *Appl. Opt.*, 26, 3838  
 Rees, D. E., & Semel, M. D. 1979, *A&A*, 74, 1  
 Rezaei, R., Schlichenmaier, R., Beck, C., & Bellot Rubio, L. R. 2006, *A&A*, 454, 975  
 Riethmüller, T.L., Solanki, S.K., & Lagg, A. 2008, *ApJ*, 678, L157  
 Rimmele, T.R. 2004, *ApJ*, 604, 906  
 Rimmele, T.R. 2008, *ApJ*, 672, 684  
 Scharmer, G.B. 2006, *A&A*, 447, 1111  
 Scharmer, G.B., Bjelksjo, K., Korhonen, T.K., Lindberg, B., & Petterson, B. 2003a, *Proc. SPIE*, 4853, 341  
 Scharmer, G.B., Dettori, P.M., Löfdahl, M.G. & Shand, M. 2003b, *Proc. SPIE*, 4853, 370  
 Scharmer, G.B., et al. 2008, *ApJ*, 689, L69  
 Schmidt, W., & Balthasar, H. 1994, *A&A*, 283, 241  
 Schüssler, M. & Vögler, A. 2006, *ApJ*, 641, L73  
 Selbing, J. 2005, Master's thesis, Stockholm Univ.  
 Sobotka, M. 1997, in *ASP Conf. Ser. 118*, 1st Advances in Solar Physics Euroconference. *Advances in Physics of Sunspots*, ed. B. Schmieder, J. C. del Toro Iniesta, & M. Vázquez (San Francisco, CA: ASP), 155  
 Sobotka, M., Bonet, J. A., & Vázquez, M. 1993, *ApJ*, 415, 832  
 Sobotka, M. & Jurčák, J. 2009, *ApJ*, 694, 1080  
 Sobotka, M. & Puschmann, K.G. 2009, *A&A*, 504, 575  
 Socas-Navarro, H., Martínez Pillet, V., Sobotka, M., & Vázquez, M. 2004, *ApJ*, 614, 448  
 Solanki, S. K., & Montavon, C. A. P. 1993, *A&A*, 275, 283  
 Uitenbroek, H. 2003, *ApJ*, 592, 1225  
 van Noort, M.J. & Rouppe van der Voort, L.H.M. 2008, *A&A*, 489, 429  
 van Noort, M., Rouppe van der Voort, L., & Löfdahl, M.G. 2005, *Sol. Phys.*, 228, 191